

## NUMERICAL SIMULATION OF FLOW FIELD IN CHEMICAL VAPOR REACTOR FOR NANOPARTICLE SYNTHESIZED

by

**Shu Jun ZHANG<sup>a\*</sup>, Wei Li WANG<sup>a</sup>, Hong Guang SUN<sup>a</sup>,  
and Dumitru BALEANU<sup>b</sup>**

<sup>a</sup> Center for Hydraulics and Fluid Mechanics, College of Mechanics and Materials,  
Hohai University, Nanjing, China

<sup>b</sup> Department of Mathematics, Cankaya University, Ankara, Turkey

Original scientific paper  
<https://doi.org/10.2298/TSCI20S1031Z>

*This paper provided a numerical simulation of fluid dynamics in the chemical vapor reactor for nanoparticle synthesis. Standard  $k-\epsilon$  turbulence equation and eddy-dissipation model with standard wall function were used to investigate the reaction process of turbulent diffusion for alumina production. Here the temperature and the operating conditions are discussed. Numerical results show that the model can well describe synthesis of nanometer alumina. The chemical reactions for alumina by this reactor are mainly concentrated in the range of 200 mm after the nozzle. The materials are completely mixed after 400 mm in the reactor.*

Key words: *chemical vapor synthesis, nanoparticles, numerical simulation*

### Introduction

Nanoparticle materials are widely used in industrial applications. Its characteristics including the particle morphology, average particle size, particle size distribution, and phase composition, has been extensively investigated. The control of these characteristics has prompted intense research into production methods of nanoparticles [1-3].

There are many investigations on the chemical and physical transformations associated with particle formation [4-6]. Zhang *et al.* [7] used scalable flame aerosol synthesis method to synthesize iron oxide nanoparticles with different size. The evolution of microstructure, phase formation, and magnetic properties during the postreduction heat treatment are systematically investigated. Analysis results show that the final particle size can be controlled by optimizing the precursor concentration and postreduction heat treatment parameters. Roth [8] studied the fundamentals of particle formation in a flame environment and further proposed a flame technology which can be used in manufacture of carbon blacks, fumed silica and transition alumina.

Chemical vapor synthesis (CVS) is one of the techniques where nanopowders are synthesized in gas phase by a chemical reaction. It is essentially a modification of chemical vapor deposition where process parameters (temperature, supersaturation, and residence time) are adjusted to form particles instead of films. As-synthesized nanopowders are usually non-agglomerated and with narrow particle size distribution by using this method [9]. In addition, many experiments were conducted in the design and operation of  $\text{Al}_2\text{O}_3$  nanopowders production. Hinklin *et al.* [10] developed an alternate synthetic approach to single and mixed-metal oxide

\* Corresponding author, e-mail: zhsj@hhu.edu.cn

nanopowders, which provides  $\text{Al}_2\text{O}_3$  nanopowders with highly hydroxylated surfaces and good dispersibility. Lukić *et al.* [11] studied direct synthesis of transition alumina nanopowders in gas phase by a chemical reaction of precursor vapor (aluminum-tri-sec-butoxide) with oxygen.

With the development of computational science, there are significant progress in the modelling and predictive simulation of complex reacting flows [12-14]. Johannessen *et al.* [15] proposed a mathematical model for the dynamics of particle growth during synthesis of ultra-fine particles in diffusion flames by solving governing equations for mass, momentum, and energy in a 2-D axisymmetric geometry. The estimated kinetics can be used to predict the surface area and shape of the particles for a wide range of synthesis conditions. Miguel *et al.* [16] simulated the flame spray pyrolysis synthesis of silica particles from volatile precursors. The CFD model couples the fluid dynamics with various processes involving precursor droplets and product particles. In flame spray pyrolysis, the design of a scalable process for synthesis of size-controlled nanomaterials was investigated to understand the role of air entrainment during their aerosol synthesis with emphasis on battery materials [17].

In this work, a numerical simulation of low filed of CVS process for producing alumina nanopowders is presented. The effects of the temperature distribution and the variation of mass fraction of  $\text{AlCl}_3$ ,  $\text{Al}_2\text{O}_3$ , and  $\text{HCl}$  are discussed.

## Governing equations

### The $k$ - $\varepsilon$ model

Turbulence must be included since eddy diffusion affects the radial transport rates in particular. The  $k$ - $\varepsilon$  model includes two extra transport equations to represent the turbulent properties of the flow, which can be expressed:

$$\rho \frac{dk}{dt} = \frac{\partial}{\partial x_i} \left[ \left( \mu + \frac{\mu_t}{\sigma_k} \right) \frac{\partial k}{\partial x_i} \right] + G_k + G_b - \rho \varepsilon - Y_M \quad (1)$$

$$\rho \frac{d\varepsilon}{dt} = \frac{\partial}{\partial x_i} \left[ \left( \mu + \frac{\mu_t}{\sigma_\varepsilon} \right) \frac{\partial \varepsilon}{\partial x_i} \right] + C_{1\varepsilon} \frac{\varepsilon}{k} (G_k + C_{3\varepsilon} G_b) - C_{2\varepsilon} \rho \frac{\varepsilon^2}{k} \quad (2)$$

where  $\varepsilon$  is the turbulent dissipation,  $k$  – the turbulent energy,  $\rho$  – the fluid density,  $G_k$  – the generation of turbulence kinetic energy due to the mean velocity gradients,  $G_b$  – the generation of turbulence kinetic energy due to buoyancy, and  $Y_M$  – the effect of compressibility to dissipation rate, the turbulent viscosity  $\mu_t$  is given:

$$\mu_t = \rho C_\mu \frac{k^2}{\varepsilon} \quad (3)$$

The standard values of all the model constants are  $C_{1\varepsilon} = 1.44$ ,  $C_{2\varepsilon} = 1.92$ ,  $C_{3\varepsilon} = 0.09$ ,  $\sigma_k = 1.0$ , and  $\sigma_\varepsilon = 1.3$ .

The inlet turbulence intensity is modeled:

$$I = 0.16 \text{Re}^{-1/8} \quad (4)$$

### Chemical reaction model

Conservation of mass species equation for component  $i$  yields:

$$\frac{\partial(\rho Y_i)}{\partial t} + \nabla(\rho \vec{v} Y_i) = -\nabla \cdot \vec{J}_i + R_i + S_i \quad (5)$$

where  $Y_i$  is the mass fraction of species  $i$ ,  $R_i$  – the net rate of production of species  $i$  per volume by chemical reactions, and  $S_i$  – the mass source. The molecular diffusive mass vector  $\vec{J}_i$  can be re-written:

$$\vec{J}_i = -\left(\rho D_{i,m} + \frac{\mu_i}{Sc_i}\right) \nabla Y_i \quad (6)$$

where  $D_{i,m}$  is the molecular diffusion coefficient for species, Schmidt number  $Sc = 0.7$ .

In the process of  $Al_2O_3$  nanoparticles production, the chemical reaction rate is controlled by turbulent mixing rate. The eddy dissipation model computes the reaction rate for reaction  $r$  as the minimum rate given by following equations:

$$R_{i,r} = v'_{i,r} M_{w,i} A \rho \frac{\varepsilon}{k} \min\left(\frac{Y_R}{v'_{R,r} M_{w,R}}\right) \quad (7)$$

$$R_{i,r} = v'_{i,r} M_{w,i} A B \rho \frac{\varepsilon}{k} \frac{\sum P Y_p}{\sum_j v'_{j,r} M_{w,j}} \quad (8)$$

where  $v'$  is the stoichiometric coefficient for reactant  $i$  in reaction  $r$ ,  $M$  – the molecular weight,  $A$  and  $B$  – the empirical constants ( $A = 4.0$ ,  $B = 0.5$ ),  $Y_R$  – the mass fraction of a particular reactant, and  $Y_p$  – the mass fraction of any product species.

### Equation of energy

The parameters such as thermal conductivity, viscosity and specific heat change with temperature in the chemical reaction process. Among these coefficients the change of specific heat with temperature is considered in the calculation. Because it has a great influence on the calculation results, while other physical parameters are set as constants [18].

The equation of energy:

$$\frac{\partial(\rho E)}{\partial t} + \nabla[\vec{v}(\rho E + p)] = \nabla\left[k_{\text{eff}} \nabla T - \sum_j h_j J_j + (\tau_{\text{eff}} \vec{v})\right] + S_h \quad (9)$$

where  $E$  is the energy,  $k_{\text{eff}}$  – the thermal conductivity, and the source term  $S_h$  denotes the rate of heat evolution from chemical reactions and radiant heat absorption. In eq. (9), the first three items on the right-hand side are energy changes due to heat conductivity, species diffusion and viscous dissipation, respectively.

Enthalpy  $h$  can be written:

$$h_j = \int_{T_{\text{ref}}}^T c_{p,j} dT \quad (10)$$

where  $T_{\text{ref}}$  and  $C_{p,j}$  are reference temperature and specific heat capacity of the species  $j$ , respectively.

## Model specification and results

### Geometric model and validation

The synthesis of nanoparticles aluminum oxide by the vapor-phase aluminum chloride is represented:



A schematic representation of the apparatus for the synthesis of alumina nanoparticle from precursors is shown in fig. 1(a). The reactor consists a heating system (similar to double-pipe heat exchang), a reactor and a post-processing device. The preheated precursors are sprayed into the reactor with an inner diameter of 50 mm and a length of 500 mm. The length of nozzle extending into the reactor is 100 mm. The outer diameter of central pipe and annular pipe are 22 mm and 44 mm, respectively.

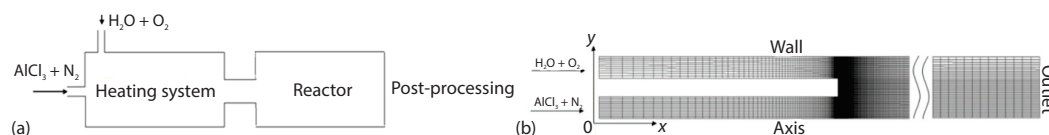


**Figure 1. Schematic representation of production of  $\text{Al}_2\text{O}_3$  nanopowder by CVS; (a) schematic representation and (b) computational grid for the react environment**

The simulation is carried out with a 2-D computational grid due to a rotational symmetry. Solid works are used for mesh structural domain illustrated in fig. 1(b). Considering that the reaction is mainly concentrated in the area near the nozzle, the gradient grid are used for mesh generation. The front and back sides are set as mass inlet and pressure outlet boundary, respectively. The inner boundary condition is set as thermally insulated.

Table 1 shows the parameters and three operating conditions used in the simulation [19]. The ratio of each precursors species is same.

**Table 1. Operating conditions for chemical reaction**

Operating conditions	$\text{AlCl}_3$ [mols $^{-1}$ ]	$\text{N}_2$ [mols $^{-1}$ ]	$\text{H}_2\text{O}$ [mols $^{-1}$ ]	$\text{O}_2$ [mols $^{-1}$ ]
1	0.03	0.12	0.2	0.1
2	0.046	0.184	0.307	0.153
3	0.1	0.4	0.667	0.333

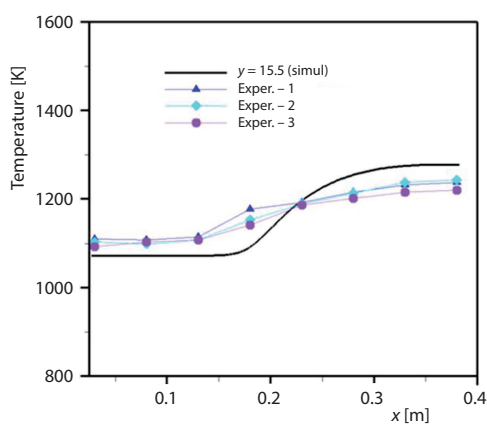
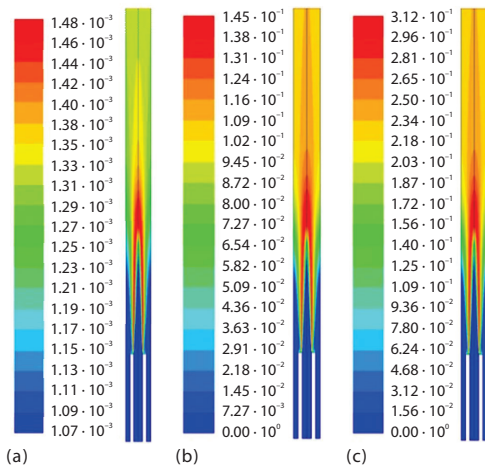


**Figure 2. Measured and simulated temperature profiles for Case 1 at  $y = 15.5$  mm**

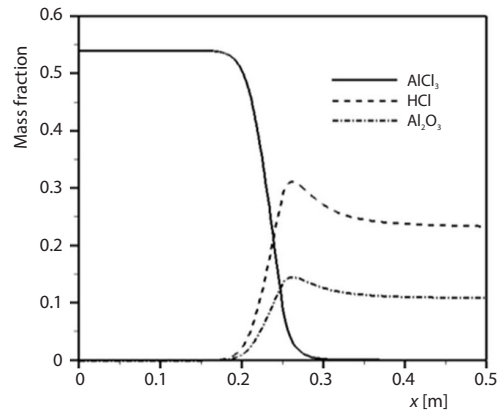
Figure 3 shows the distribution of temperature and mass fraction of  $\text{Al}_2\text{O}_3$  and  $\text{HCl}$  in the reactor. It is noted that the high mass fraction of  $\text{Al}_2\text{O}_3$  and  $\text{HCl}$  is agreement with the high temperature. This means that gas-phase species mixing is enhanced with the temperature, and as a result, the rate of the chemical reactions is increased.

## Results and discussions

The temperature at 1.5 mm from the inner wall is measured by a thermocouple inserted in a glass pocket extending into the reactor when the reaction is stable. Three sets of measured and calculated temperatures are compared on fig. 2. With the inlet preheated precursors gas above 800 °C, the temperature increases at 100 mm from the end of nozzle. Due to the difficulty of measuring precisely with a thermocouple in the extreme environment, deviation between measurement and simulation is acceptable. We consider the agreement between measurements and simulation in fig. 1 a good validation of the calculated temperature field.



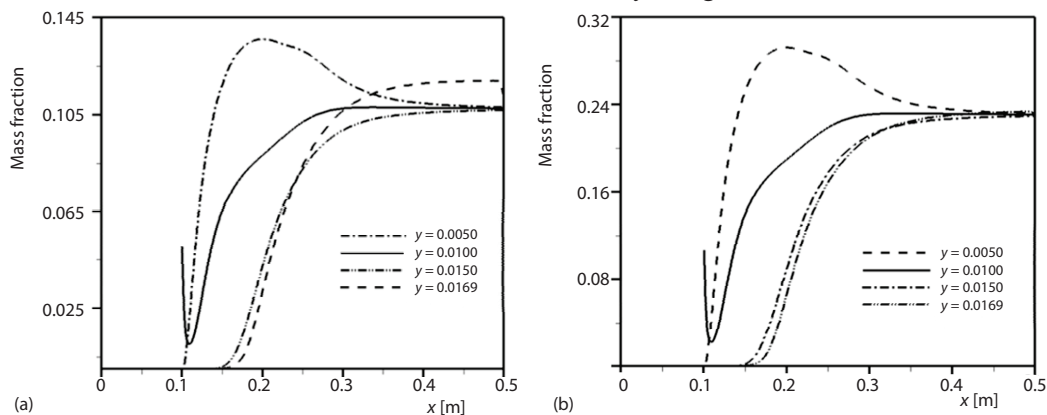
**Figure 3.** Contours of temperature and mass fraction of  $\text{Al}_2\text{O}_3$  and HCl in the entire reactor (Case 1); (a) temperature [K], (b)  $\text{Al}_2\text{O}_3$ , and (c) HCl



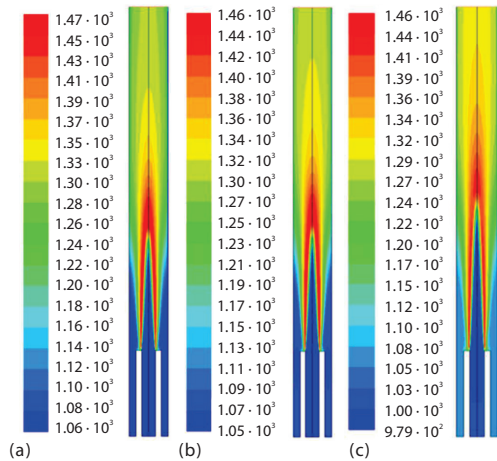
**Figure 4.** The variation of mass fraction of  $\text{AlCl}_3$ ,  $\text{Al}_2\text{O}_3$ , and HCl along the center axis

Figure 4 depicts the variation of mass fraction of  $\text{AlCl}_3$ ,  $\text{Al}_2\text{O}_3$  and HCl along the center axis. It is shown that with the production of  $\text{Al}_2\text{O}_3$ ,  $\text{AlCl}_3$  are consumed rapidly at about 200 mm in the axial direction, the synthesis completes at 300 mm. At this point, all the precursor species are consumed and the reaction area is about 200 mm.

The variation of mass fraction of  $\text{Al}_2\text{O}_3$  and HCl along the radial direction are shown in fig. 5. It can be observed that  $\text{Al}_2\text{O}_3$  is synthesized at  $y = 0.005$  m (the inner edge of the central pipe) at  $x = 100$  mm (*i. e.* the nozzle outlet) and increased rapidly from  $x = 100$ -200 mm, then the mass fraction decrease due to diffusion and finally tended to a certain level, fig. 5(a). Because of the dilution by the mixture of water vapor and oxygen at the center pipe outlet, the mass fraction of  $\text{Al}_2\text{O}_3$  in the surface near the outer edge of the central pipe ( $y = 0.010$  m) decreases and rises later. The  $\text{Al}_2\text{O}_3$  mass fraction gradually increases and approaches to a higher magnitude than the other three positions at  $x = 250$  mm near the wall ( $y = 0.0169$  m). The mass fraction curve of HCl is similar to that of  $\text{Al}_2\text{O}_3$  except that of  $y = 16.9$  mm. It can be seen from fig. 5(b) that the mass fraction of HCl in the reaction device tends to the same level at  $x = 400$  mm, which indicates that HCl is mixed uniformly along the radial direction.



**Figure 5.** The variation of mass fraction of  $\text{Al}_2\text{O}_3$  and HCl along the radial direction; (a)  $\text{Al}_2\text{O}_3$ , (b) HCl



**Figure 6. Contours of gas temperature [K] in the reactor; (a) Case 1, (b) Case 2, and (c) Case 3**

of  $\text{Al}_2\text{O}_3$  decrease with inlet flow rate. It is also illustrated that high mass fraction of  $\text{Al}_2\text{O}_3$  correspond to low temperature near the wall by a comparison between figs. 7(a) and 7(b).

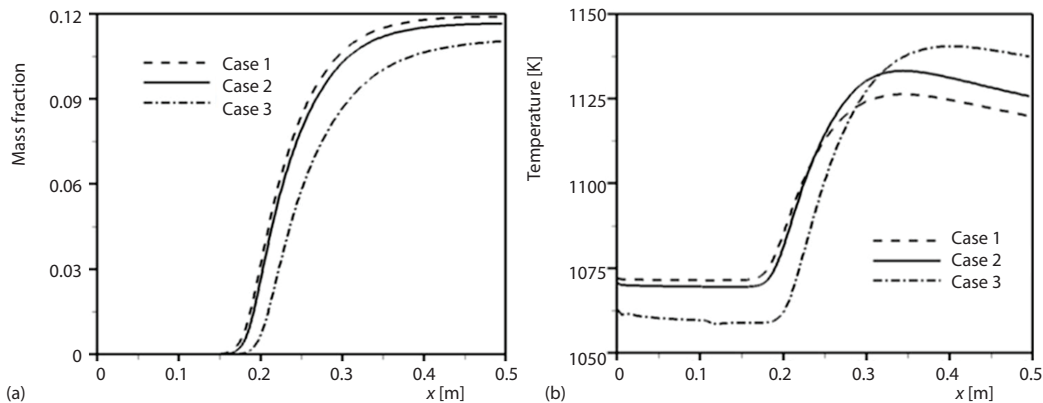


**Figure 7. Simulation results of temperature profiles and mass fraction of  $\text{Al}_2\text{O}_3$  at  $y = 16.9$  mm; (a) mass fraction and (b) temperature [K]**

## Conclusion

This paper employs the method of CVS, standard  $k-\varepsilon$  turbulence model, eddy-dissipation model and standard wall function numerically simulate the reaction process of turbulent diffusion for  $\text{Al}_2\text{O}_3$  nanoparticle production. The model is validated by experimental measurement of temperature. With the production of  $\text{Al}_2\text{O}_3$ ,  $\text{AlCl}_3$  are consumed rapidly at about 200 mm in the axial direction, and the synthesis of nanometer  $\text{Al}_2\text{O}_3$  are mainly concentrated in the range of 200 mm after the nozzle. The high temperature areas of Capacity 3 are delayed for a certain distance due to the highest inlet flow rate. The mass fraction of  $\text{Al}_2\text{O}_3$  decrease with inlet flow rate. It is also illustrated that high mass fraction of  $\text{Al}_2\text{O}_3$  corresponds to low temperature near the wall.

Figure 6 shows the effect of the inlet flow rate on the gas temperature. The initial temperature at the inlet is 1073 K. It is noted that the temperature increases correspondingly due to chemical reaction. The reaction high temperature areas of Case 1 and Case 2 are basically in the same area, while the high temperature areas of Case 3 are delayed for a certain distance due to the highest inlet flow rate. The distribution of temperature for three capacities are different at end of the reaction device.

The profiles of temperature and mass fraction of  $\text{Al}_2\text{O}_3$  at  $y = 16.9$  mm are shown in fig. 7. It can be seen from the fig. 7(a) that the initial position of product  $\text{Al}_2\text{O}_3$  diffusion near the wall is very close under the three production capacity conditions. The mass fraction of  $\text{Al}_2\text{O}_3$  decrease with inlet flow rate.

## Acknowledgment

This research was funded by the National Natural Science Foundation of China, grant numbers 11972148, 11811530069 and Natural Science Foundation of Jiangsu Province, P.R. China Grant No. BK20190024.

## References

- [1] Jang, H. D., *et al.*, Synthesis of SiO<sub>2</sub> Nanoparticles from Sprayed Droplets of Tetraethyl Orthosilicate by the Flame Spray Pyrolysis, *Current Applied Physics*, 6 (2006), Suppl. 1, pp. 110-113
- [2] Grohn, A. J., *et al.*, Fluid-Particle Dynamics During Combustion Spray Aerosol Synthesis of ZrO<sub>2</sub>, *Chemical Engineering Journal*, 191 (2012), May, pp. 491-502
- [3] Martín, M. I., *et al.*, Microstructural and Morphological Analysis of Nanostructured Alumina Particles Synthesized at Low Temperature via Aerosol Route, *Journal of the European Ceramic Society*, 28 (2008), 13, pp. 2487-2494
- [4] Martín, M. I., *et al.*, Nanostructured Alumina Particles Synthesized by the Spray Pyrolysis Method: Microstructural and Morphological Analyses, *Ceramics International*, 36 (2010), 2, pp. 767-772
- [5] Buesser, B., Pratsinis, S. E., Design of Nanomaterial Synthesis by Aerosol Processes. *Annual Review of Chemical and Biomolecular Engineering*, 3 (2012), Feb., pp. 103-127
- [6] Karatas, A. E., Gulder, O. L., Soot Formation in High Pressure Laminar Diffusion Flames, *Progress in Energy and Combustion Science*, 38 (2012), 6, pp. 818-845
- [7] Zhang, Z. L., *et al.*, Synthesis of Ultrafine Iron Powder by Combining the Flame Aerosol Synthesis and Postreduction, *Journal of Materials Research*, 34 (2019), 23, pp. 3964-3974
- [8] Roth, P., Particle Synthesis in Flames, *Proceedings of the Combustion Institute*, 31 (2007), 2, pp. 1773-1788
- [9] Wintere, M., *Nanocrystalline Ceramics – Synthesis and Structure*, Springer Verlag, Berlin, Germany, 2002
- [10] Hinklin, T., *et al.*, Liquid-Feed Flame Spray Pyrolysis of Metalloorganic and Inorganic Alumina Sources in the Production of Nanoalumina Powders, *Chemistry of Materials*, 16 (2004), 1, pp. 21-30
- [11] Lukić, S., *et al.*, Chemical Vapor Synthesis and Characterization of Al<sub>2</sub>O<sub>3</sub> Nanopowders, *Ceramics International*, 41 (2015), 3, Part A, pp. 3653-3658
- [12] Ji, Y., *et al.*, Computational Fluid Dynamic Modelling of a Flame Reaction Process for Silica Nanopowder Synthesis from Tetraethyl Orthosilicate, *Journal of the American Ceramic Society*, 90 (2007), 12, pp. 3838-3845
- [13] Buesser, B., Grohn, A. J., Multiscale Aspects of Modelling Gas-Phase Nanoparticle Synthesis, *Chemical Engineering and Technology*, 35 (2012), 7, pp. 1133-1143
- [14] Buesser, B., Pratsinis, S. E., Design of Gas-Phase Synthesis of Core-Shell Particles by Computational Fluid Aerosol Dynamics, *AIChE Journal*, 57 (2011), 11, pp. 3132-3142
- [15] Johannessen, T., *et al.*, Computational Fluid-Particle Dynamics for the Flame Synthesis of Alumina Particles, *Chemical Engineering Society*, 55 (2000), 1, pp. 177-191
- [16] Miguel, O. M., *et al.*, Computational Fluid Dynamic Modelling of the Flame Spray Pyrolysis Process for Silica Nanopowder Synthesis, *Journal of Nanoparticle Research*, 17 (2015), 7, 324
- [17] Oliver, W., *et al.*, Process Design for Size-Controlled Flame Spray Synthesis of Li<sub>4</sub>Ti<sub>5</sub>O<sub>12</sub> and Electrochemical Performance, *Chemical and Process Engineering*, 38 (2017), Mar., pp. 51-66
- [18] Wang, L. X., *et al.*, Analysis of Factors Affecting Simulation of Turbulent Diffusion Combustion, *China Powder Science and Technology*, (2005), 1, pp. 16-20
- [19] Ye, D. L., *Handle of Applied Inorganic Thermodynamic Data*, 2<sup>th</sup> Ed., (in Chinese), Beijing Metallurgical Industry Press, Beijing, China, 2002, pp. 63-72